

Article

Malonaldehyde-like Systems: BeF₂ Clusters—A Subtle Balance between Hydrogen Bonds, Beryllium Bonds, and Resonance

M. Merced Montero-Campillo , Otilia Mó  and Manuel Yáñez * 

Departamento de Química, Módulo 13, Facultad de Ciencias and Institute of Advanced Chemical Sciences (IAdChem), Universidad Autónoma de Madrid, Campus de Excelencia UAM-CSIC, Cantoblanco, 28049 Madrid, Spain; mm.montero@uam.es (M.M.M.-C.); otilia.mo@uam.es (O.M.)

* Correspondence: manuel.yanez@uam.es

Abstract: The stability of malonaldehyde is governed by intramolecular hydrogen bonds (IMHBs) as well as in malonaldehyde-like systems where oxygen is replaced by N or S at any of the basic sites. As beryllium bonds have been shown to strongly cooperate with hydrogen bonds, this work explores at the high level ab initio G4 level of theory the effect of including this non-covalent interaction in the system through its association with BeF₂. Although malonaldehyde follows the expected trends, where the formation of a pseudocyclic form is favored also when IMHB and Be bonds are present, the subtle balance between both non-covalent interactions leads to some surprising results when other heteroatoms are involved, to the point that interaction energies can be much larger than expected or even cyclization is not favored. A complete analysis using different computational tools gives an answer to those cases escaping the predictable trends.

Keywords: intramolecular hydrogen-bonds; beryllium bonds; cooperativity; resonance



Citation: Montero-Campillo, M.M.; Mó, O.; Yáñez, M. Malonaldehyde-like Systems: BeF₂ Clusters—A Subtle Balance between Hydrogen Bonds, Beryllium Bonds, and Resonance. *Sci* **2022**, *4*, 7. <https://doi.org/10.3390/sci4010007>

Academic Editor: Styte M. Antao

Received: 20 November 2021

Accepted: 2 February 2022

Published: 13 February 2022

Publisher's Note: MDPI stays neutral with regard to jurisdictional claims in published maps and institutional affiliations.



Copyright: © 2022 by the authors. Licensee MDPI, Basel, Switzerland. This article is an open access article distributed under the terms and conditions of the Creative Commons Attribution (CC BY) license (<https://creativecommons.org/licenses/by/4.0/>).

1. Introduction

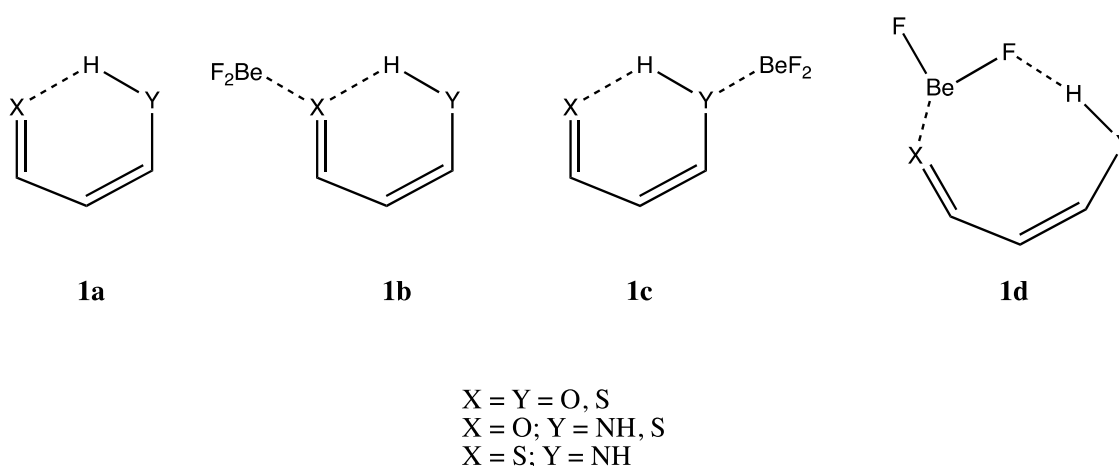
Non-covalent interactions play a fundamental role in practically all realms of chemistry. Johannes Diderik van der Waals was the first scientist that at the end of the 19th century, concluded that the peculiar behavior of real gases, which did not follow strictly the ideal gases laws, was actually due to the existence of attracting forces between the molecules that made up the gas, that later on would be named van der Waals forces in his honor [1]. Since then, the interest in this new type of forces has been growing and growing. A second milestone in this field was the characterization of hydrogen bonds, a new and specific non-covalent interaction responsible, for instance, for the liquid state of water at room temperature. In the words of Linus Pauling in 1935 [2], “It has been recognized since the discovering of the hydrogen bond [3] that the natural properties of water and ice (. . .) owe their existence to hydrogen bonds between water molecules”. It would be Linus Pauling himself who would show, for the first time, that hydrogen bonds were also responsible for the helical structure of proteins [4]. One century after the van der Waals PhD thesis, the fundamental role of different non-covalent interactions was evident in an impressive number of phenomena in the realm of chemistry [5–8], physics [9], catalysis [10–14], biochemistry [15–19], and material sciences [20–23].

During the last decade of the 20th century and the first two decades of the 21st century, new types of these non-covalent interactions (NCIs) and their characterization were reported year after year. Among them, aerogen [24], halogen [25,26], chalcogen [27–30], tetrel [31,32], triel [33,34], spodium [35], regium or coinage-metal [36–39], alkaline-earth [40,41], and alkaline-bonds [42] have been described. Beryllium bonds [43,44], a subfamily of the alkaline-earth NCIs, were characterized more than a decade ago [43] and after then, the attention on them has grown in a very significant way [45–50].

One of the most interesting signs of identity of non-covalent interactions is cooperativity [51,52]. For instance, this phenomenon is responsible for the cyclic structure of the water

trimer [53], where all three hydrogen bonds are stronger than in the water dimer. Similar cooperative effects are also characteristic of methanol, water, and formaldehyde clusters [54] and are again observed between halogen bonds stabilizing long linear chains [55].

However, cooperativity can enhance other weak interactions [56] by favoring the interplay between non-covalent interactions of different nature, such as hydrogen and halogen bonds [57–59], hydrogen, halogen, and beryllium bonds [46], hydrogen and tetrel bonds [60], hydrogen and tetrel bonds modulated by magnesium bonds [61], tetrel and beryllium bonds [62], halogen, chalcogen, and pnictogen bonds [63], pnictogen and beryllium bonds [64], halogen and beryllium bonds [45], or chalcogen and alkaline-earth bonds [41]. Although the cooperativity between beryllium bonds and intermolecular hydrogen bonds has been investigated [65], the interplay between beryllium bonds and intramolecular hydrogen bonds is still an open question, where unavoidably, the electron density redistribution associated with both non-covalent interactions occur in just the molecule exhibiting the intramolecular hydrogen bond (IMHB). A paradigmatic case of IMHB is malonaldehyde, in which the formation of the hydrogen bond has been identified with a resonance assisted phenomenon [66]. For this reason, we selected malonaldehyde and malonaldehyde-like systems (Scheme 1a) interacting with BeF_2 (Scheme 1b–d) to investigate the electron density redistribution and cooperativity between IMHB and Be bonds. The IMHB might be formed as in the isolated malonaldehyde-like system (six-membered ring, Scheme 1b,c) or mediated by one F atom of the BeF_2 molecule (eight-membered ring, Scheme 1d). In structures Scheme 1b,c, the beryllium bond is formed between the lone pairs of one of the heteroatoms, acting as a Lewis base, and the beryllium atom, acting as a Lewis acid, resulting in two possible binding sites per molecule. Therefore, our survey allows covering IMHBs and beryllium bonds of different strength.



Scheme 1. Malonaldehyde and malonaldehyde-like derivatives are compared to the same systems upon interaction with BeF_2 in different X or Y binding sites.

2. Computational Details

A correct description of non-covalent interactions usually requires employing high-level *ab initio* methods because the corresponding binding energies are much smaller than those of conventional chemical bonds, and therefore, the errors in obtaining them should be reduced as much as possible. Although Be bonds are usually stronger than other non-covalent interactions [43,44], they are still weaker than most of the conventional chemical bonds, and therefore, the use of high-level *ab initio* calculations is still advisable. On top of that, the adequate description of the bonding in Be bonds requires a correct treatment of the electron correlation effects [43,44]. Hence, for all these reasons, we have decided to use in our survey the high-level *ab initio* Gaussian-4 (G4) theory [67]. The G4 theory is a composite method based on the combination of energy components obtained at MP2, MP4 [68,69], and CCSD(T) [70] levels of theory, and a final correction to the

Hartree–Fock limit. The final energies will be very close to the ones obtained if a formal CCSD(T,full)/G3LargeXP calculation is employed. In this composite method, the equilibrium structures are optimized at the B3LYP/6-31G(2df,p) level. The same level is used to calculate the harmonic frequencies and the different terms to obtain from the G4 final energies the enthalpies and free energies. In general, the G4 thermochemistry magnitudes have an average absolute deviation from the experiment of $3.47 \text{ kJ}\cdot\text{mol}^{-1}$ [67]. For some specific cases, we carried out IRC (intrinsic reaction coordinate) additional calculations to better characterize the typical proton transfer in malonaldehyde-like systems connecting two minima. The potential energy curves obtained by this method were obtained at the B3LYP/6-31G(2df,p) level of theory.

To understand the factors behind the stability of the aggregates investigated, a good analysis of the changes in the electron density distribution of the malonaldehyde-like system is required, because these density redistributions may be crucial to understand the stability of the complex. This analysis is rather complete if three different, but at the same time, complementary approaches are used, namely the Quantum Theory of Atoms in Molecules (QTAIM) [71], the natural bond orbital (NBO) analysis [72], and the electron density shifts (EDS) [73]. The QTAIM method is based on an analysis of the topology of the electron density of the system through the location of its critical points, in particular the bond critical points (BCPs) whose electron density, ρ , is a measure of the strength of the interaction between two connected atoms, independently of the nature of the interaction. This method also provides an estimation of the atomic charges, which are the ones used in some specific points of the analysis. The NBO method permits, through the calculation of second-order orbital interaction energies, to characterize electron donations and back-donations among localized hybrid orbitals of the interacting molecules and to obtain the natural atomic charges that result from these donations and back-donations. It also allows evaluating the Wiberg bond index, ref. [74], which provides a clear indication of the strength of a linkage. Finally, the EDS is obtained as the difference of the electron density of the complex and the isolated monomers in the geometry of the complex and permits identifying which areas of the electron donor are preferentially depopulated and which areas of the Lewis acid are preferentially populated [75].

3. Results and Discussion

As explained in the Introduction, we have analyzed in our theoretical survey the structure and stability of all the complexes in which the BeF_2 molecule interacts with the different basic sites of the malonaldehyde-like compounds investigated (Scheme 1). As the presence of the IMHB is key for the system, we took as a starting point the linear and pseudocyclic conformations of the isolated systems. These conformers can be compared to the linear and pseudocyclic conformations of the BeF_2 -containing complexes, thus allowing to see the influence of the Be bond in the IMHB.

3.1. $X = Y = \text{O}, \text{S}$

Figure 1 shows the different structures obtained for malonaldehyde, the reference system, and its dithio analogue. For all the other malonaldehyde-like derivatives, this information is provided in Figures S1–S3 of the Supporting Information. Note that the linear and pseudocyclic isolated systems are shown in the first row, where the IMHB distances are 1.646 \AA ($X = \text{O}$) and 2.102 \AA ($X = \text{S}$).

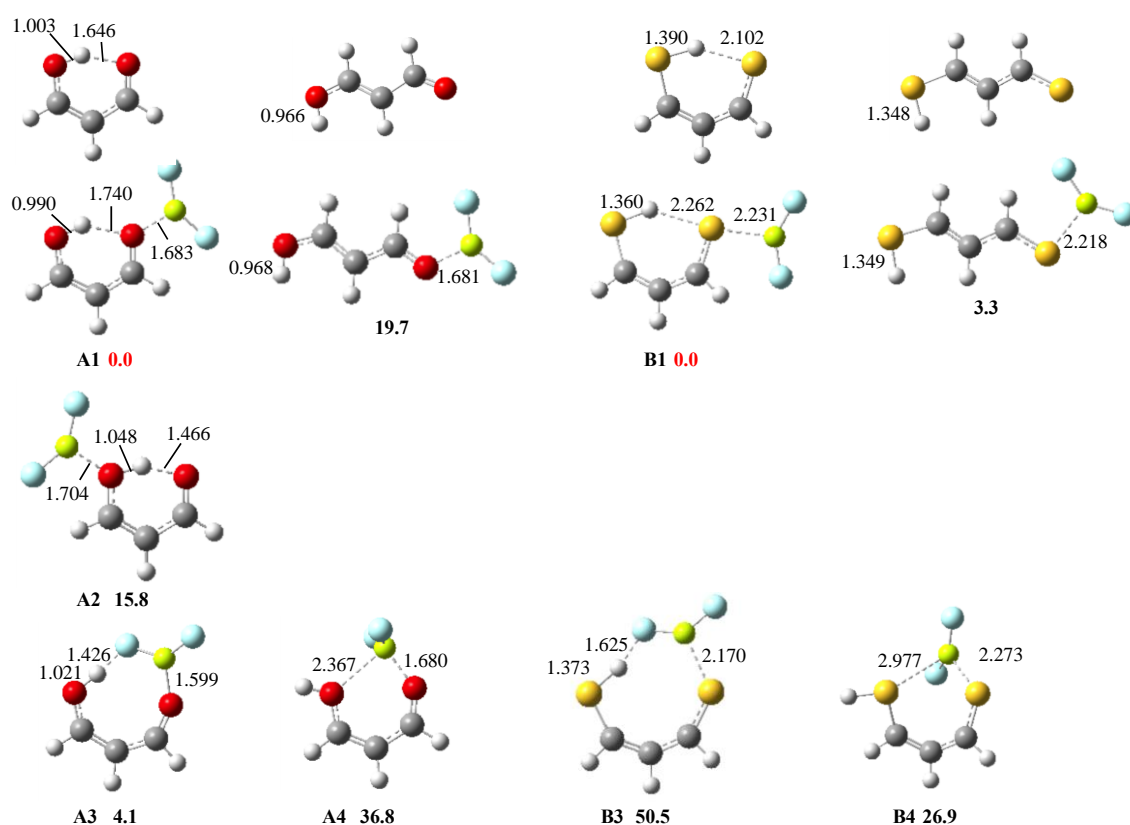


Figure 1. Optimized structures of the complexes between malonaldehyde and its dithio derivative with BeF₂, showing the relative enthalpies (in kJ·mol⁻¹) with respect to the global minimum (in red). Bond lengths are in Å. Atom color code: C, gray; H, white; O, red; S, mustard yellow; Be, lemon yellow; F, light blue.

The first conspicuous fact is that for both, malonaldehyde and its dithio analogue, the global minima, **A1** and **B1**, respectively, correspond to the association of BeF₂ to the C=O (C=S) group, which is the most basic site of these compounds. However, there is a difference when the attachment takes place at the OH group. As shown in Figure 1, for malonaldehyde, the corresponding cluster, **A2**, is found to be 15.8 kJ·mol⁻¹ higher in energy than the global minimum. A comparison of the molecular graphs of these two minima (see Figure 2), and in particular the electron density at the O-H···O BCP, shows that the IMHB is stronger in **A2**, with an electron density of 0.087 a.u. vs. 0.043 a.u. This is due to the formation of the Be···OH bond, which implies a significant charge transfer of 0.37 e⁻ from the malonaldehyde to the empty orbitals of Be. Such a charge transfer is reflected in the atomic charge of the O atom, which is much more negative (−0.36) in the isolated malonaldehyde than in its complex with BeF₂ (−0.17). The obvious consequence is an increase in the positive charge of the H atom attached to the oxygen (from +0.33 in the isolated malonaldehyde to +0.36 in the cluster with BeF₂). This implies an acidity increase in the OH group and, as a consequence, the reinforcement of the O-H···O IMHB. Consistently, the NBO analysis shows that second-order interaction energies associated to the O-H···O IMHB are three times larger in **A2** (284 kJ·mol⁻¹) than in **A1** (79 kJ·mol⁻¹). A similar decrease (from 0.194 to 0.074) is observed in the corresponding Wiberg bond indexes. Nevertheless, the reinforcement of the IMHB does not counterbalance the weakening of the O···Be bond, whose electron density at the BCP decreases from 0.063 to 0.057 a.u., which is due to the fact that the hydroxyl group is a much weaker Lewis base than the carbonyl one. Again, this weakening is also reflected in the corresponding Wiberg bond index, which decreases from 0.114 to 0.097. In addition, consistently, the NBO analysis shows that the second-order interaction energy associated with the formation of the beryllium bond in **A2**

($154 \text{ kJ}\cdot\text{mol}^{-1}$) is significantly lower than in **A1** ($218 \text{ kJ}\cdot\text{mol}^{-1}$). This finding is consistent with the values of the Wiberg bond index that in the first case is 0.224, whereas in the latter, it is 0.284.

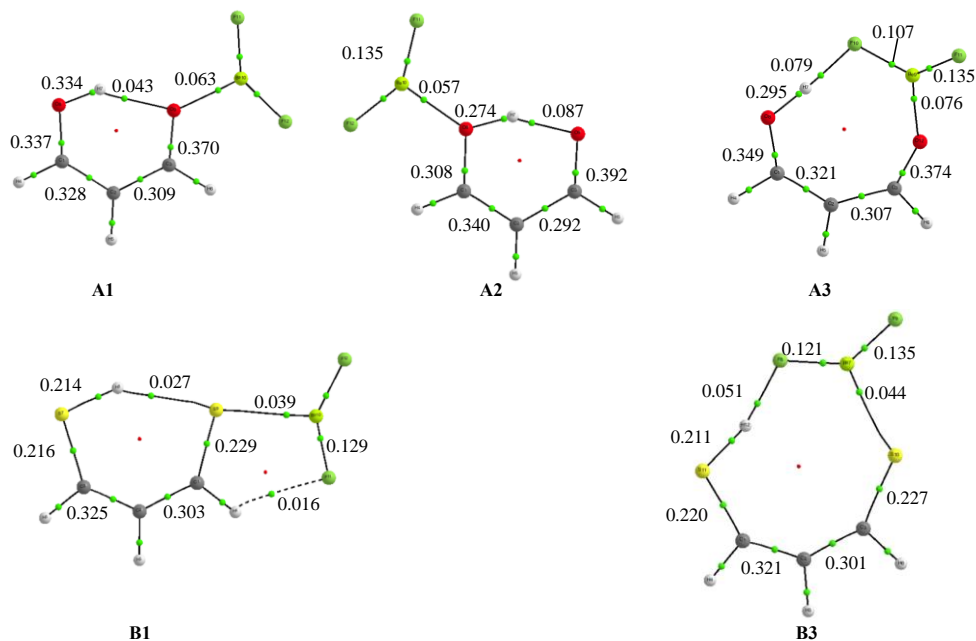


Figure 2. Molecular graphs of the complexes in which the BeF_2 molecule is attached to the carbonyl (**A1,A3**) and the hydroxyl oxygen atoms (**A2**) of malonaldehyde. Conformers (**B1,B3**) for dithiomalonaldehyde are also shown. Note that conformer (**B2**) does not exist for dithiomalonaldehyde because upon the attachment of BeF_2 to the SH group, a spontaneous proton transfer occurs, yielding conformer (**B1**). The electron densities (in a.u.) at the different BCPs (green dots) are also given.

As we have already mentioned in the Introduction, we cannot forget that the cyclization of malonaldehyde has been shown to be a paradigmatic example of what is usually called a resonance-assisted hydrogen bond (RAHB) [66], although the nature of this phenomenon was a subject of debate [76–82]. In order to assess the possible role of electron delocalization phenomena, we have used the EDS formalism described in previous sections. In Figure 3, we show the results obtained for the malonaldehyde- BeF_2 cluster. In its linear conformation, the formation of the beryllium bond is accompanied by an electron density redistribution mostly on the carbonyl group of the malonaldehyde moiety, with small changes on carbon and oxygen from the hydroxyl group. The BeF_2 is now linked to the chain through a newly populated region (violet lobes). We observe almost the same pattern for the pseudocyclic form, where the formation of the beryllium bond again modifies the densities of the carbonyl group and BeF_2 , because the participation of the carbonyl group in the $\text{O-H}\cdots\text{O}$ IMHB necessarily modulates its interaction with the BeF_2 molecule. Therefore, the important conclusion is that the carbon chain of malonaldehyde is similarly modified in both cases; i.e., resonance should be very similar in the linear and the pseudocyclic structures.

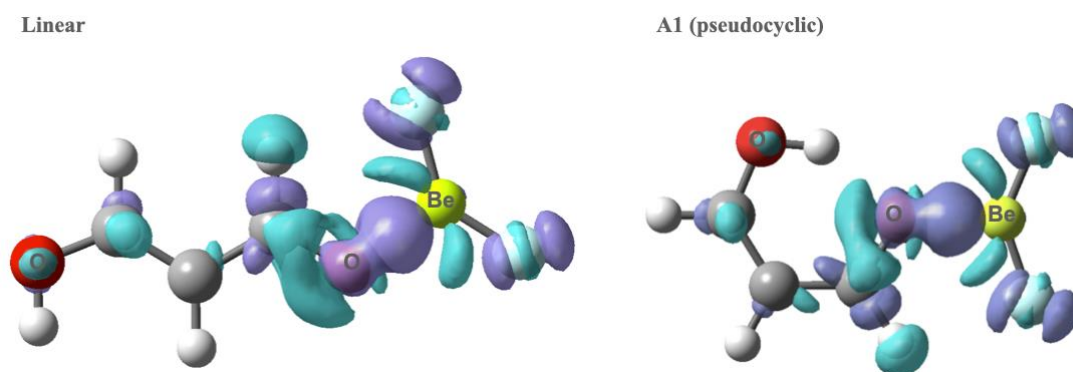


Figure 3. EDS plot for the linear and pseudocyclic conformations of the malonaldehyde-BeF₂ cluster. Violet lobes correspond to areas in which the electron density is accumulated, whereas light blue ones correspond to areas where the electron density is depleted.

For the corresponding dithio derivative, the acidity enhancement of the SH group upon association with the BeF₂ molecule is such that a local minimum **B2** analogous to **A2** does not exist because a spontaneous proton transfer takes place, so that the structure collapses to the global minimum **B1**.

A different orientation of the BeF₂ with respect to the aldehyde molecule when attaching to the C=O (C=S) group can lead, alternatively, to a local minimum, in which the OH···O (SH···S) IMHB is replaced by a OH···F (SH···F) IMHB (clusters **A3** and **B3**). These minima exhibit the strongest beryllium bond of all the local minima found, as it is clearly reflected looking at the corresponding electron densities at the BCP (see Figure 2). On top of that, the OH···F (SH···F) hydrogen bonds are also rather strong, with electron densities notably higher than those found for the OH···O (SH···S) IMHBs. However, both local minima are found to be 4.1 and 50.5 kJ·mol⁻¹ higher (not lower) in energy than the corresponding global minima. This finding reflects that, besides the two non-covalent interactions, the IMHB and the beryllium bond, a third factor also contributes to the stability of the complex. This factor is the electron delocalization in the corresponding cycle, which is clearly larger in the global minima, **A1** and **B1**, than in structures **A3** and **B3**. The energy gap in the case of the thio derivative is much larger than on the oxygen-containing analogue, because there is an additional F···H-C IMHB in the global minimum **B1** that is not present in the **B3** conformer.

Finally, it is worth noting that the coordination of Be with the two oxygen (sulfur) atoms (structures **A4** and **B4** in Figure 1) also leads to a local minimum but higher in energy than the global minimum.

The effects of the formation of a beryllium bond on energy are nicely revealed if we use thermodynamic cycles such as those shown in Figure 4, where we can evaluate the impact of cyclization and the two NCIs involved at a glance.

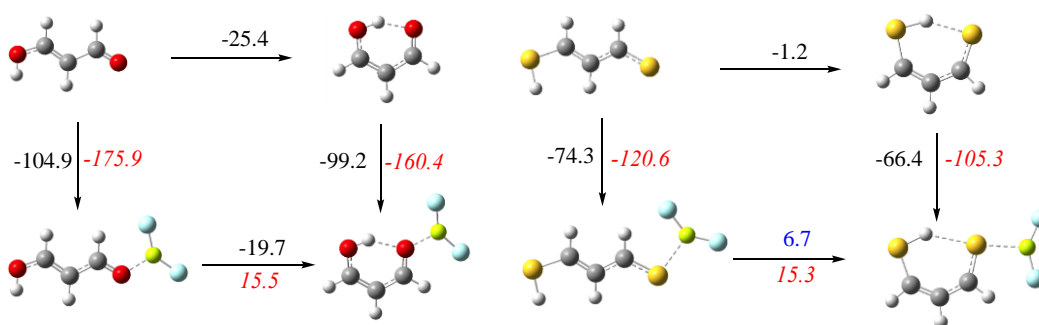
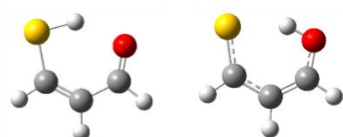


Figure 4. Thermodynamic cycles corresponding to the attachment of BeF₂ to linear and pseudocyclic malonaldehyde (**left**) and to its dithio analogues (**right**). The equilibrium interaction energies are in black if the process is exothermic and in blue if it is endothermic. The diabatic interaction energies are in red. All values in kJ·mol⁻¹.

The first conspicuous fact is that BeF₂ attachment to the cyclic aldehyde is about 6 kJ·mol⁻¹ less exothermic than the attachment to the linear one, and the O-Be bond formed is slightly weaker, the charge transferred to the BeF₂ molecule being also slightly smaller. Nevertheless, the cyclic cluster is more stable than the linear one as a consequence of the formation of the IMHB. This IMHB is also weaker than in the isolated malonaldehyde, because now, the carbonyl oxygen is participating simultaneously in the IMHB and in the beryllium bond. To well understand these apparent contradictory results, it must be taken into account that the formation of the beryllium bond involves a substantial structural distortion of both the aldehyde and the BeF₂ molecule. To quantify the energetic effects of these geometric distortions, we have included in the same figure (red numbers) the diabatic interaction energies, i.e., the energies obtained by subtracting from the energy of the complex the energy of the two interacting systems with the geometry they have in the complex. The first important feature is that these interaction energies are substantially larger than the adiabatic ones, indicating that the geometry deformation of the interacting systems is large. The second important finding is that in terms of the diabatic energies, the formation of the beryllium bond is now less exothermic in the cyclic than in the linear structure, because, as we have mentioned above, in the latter case, the oxygen atom is a poorer basic center than in the first case, as it is also involved in the IMHB. Consistently, the IMHB in the complex is necessarily weaker than the isolated malonaldehyde. The situation is qualitatively similar, but quantitatively different, when looking at the dithio derivative. In this case, the formation of the IMHB is only slightly exothermic and becomes slightly endothermic upon interaction with BeF₂. This is the expected behavior considering the donor abilities of oxygen and sulfur.

3.2. X = O, Y = S

In this particular case, if we take into account that there are two stable isomers (see Scheme 2), there are in principle four possible binding sites for the attachment of BeF₂: (a) the carbonyl group, (b) the SH group, (c) the OH group, and (d) the thiocarbonyl group. However, they reduce to three because the attachment to the SH group is followed by a spontaneous proton transfer to yield the enolic form.



Scheme 2. The two possible isomers for X = O, Y = S.

For the sake of conciseness, we are not going to discuss here the geometrical features of these systems, although the optimized structures are provided in Figure S1 of the

Supporting Information. In Figure 5, we present the corresponding thermodynamic cycles corresponding to the BeF_2 association to the carbonyl, to the thiocarbonyl, and to the hydroxyl group, respectively.

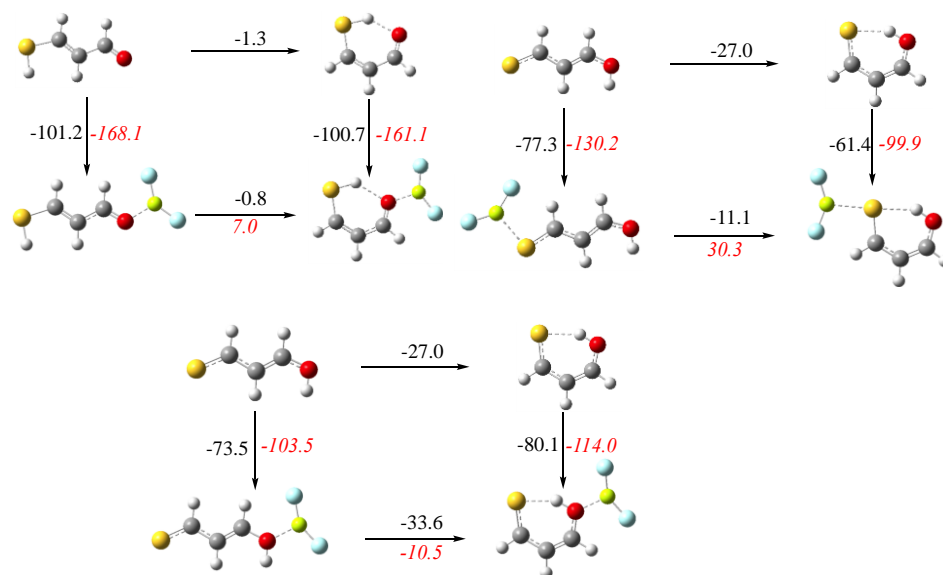


Figure 5. Thermodynamic cycles corresponding to the attachment of BeF_2 to the malonaldehyde-like in which its hydroxyl group has been replaced by a thiohydroxyl one. In black, equilibrium interaction energies, and in red, diabatic values. All values in $\text{kJ}\cdot\text{mol}^{-1}$.

In the first two cases, the situation is similar to the one we have already discussed in Figure 4 for malonaldehyde and its dithio analogue, in the sense that the formation of the beryllium bond results in both cases in a weakening of the IMHB. The weakening is very small when Be is attached to the carbonyl group (global minimum), because the IMHB was already rather weak in the isolated thioaldehyde, as the SH is a poor proton donor. When Be is attached to the thiocarbonyl group, the weakening of the IMHB is remarkably larger, because an excellent Lewis acid such as BeF_2 is able to withdraw a significant amount of electron density from sulfur, which is consequently a much worse donor toward the OH group. Indeed, whereas the Wiberg bond index for the $\text{O}\cdots\text{S}$ IMHB in the isolated thiomalonaldehyde is 0.192, in the complex with BeF_2 , it is only 0.110.

However, a surprising result is observed when Be attachment occurs at the hydroxyl group. In contrast with all previous cases, the formation of the $\text{OH}\cdots\text{S}$ IMHB is more exothermic than in the isolated molecule (33.6 vs. 27.0 $\text{kJ}\cdot\text{mol}^{-1}$). This is also ratified by an analysis of the electron density at the BCP, which shows indeed that the IMHB is notably stronger in the BeF_2 -containing cluster than in the isolated compound (0.056 vs. 0.045 a.u., see Figure 6).

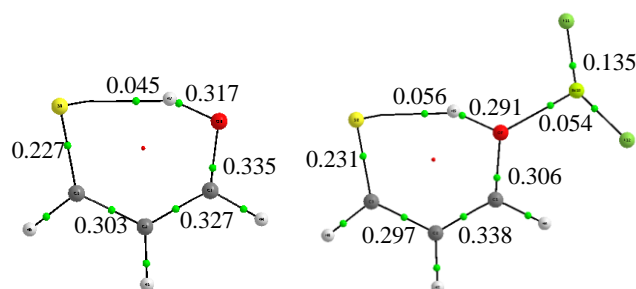


Figure 6. Molecular graphs of the malonaldehyde-like system for $X = \text{O}$, $Y = \text{S}$, and its complex with BeF_2 attached to the hydroxyl oxygen atom, showing that this system presents a stronger $\text{O}\cdots\text{S}$ IMHB in the Be-bond containing structure. Electron densities at the BCPs (green dots) in a.u.

The same conclusion is reached when looking at the NBO results, which show that the second-order interaction energy associated to the O-H...S IMHB is 1.5 times larger in the BeF₂ complex than in the isolated molecule, and that the O-H...S Wiberg bond index goes from 0.192 to 0.263 upon attachment of BeF₂ to the OH group. However, not only the IMHB becomes reinforced; the beryllium bond is stronger as well. Indeed, an analysis of the charge distribution also reveals that whereas in the linear complex, with no IMHB, the charge transfer from the thiomalonaldehyde toward the BeF₂ molecule is 0.33 e⁻, whereas in the cyclic conformer, this charge transfer is 0.35 e⁻. Consistently, in the latter case, the O...Be distance is 0.003 Å shorter. A plausible explanation is that in this particular case, the oxygen involved in the Be bond in the pseudocyclic form is a proton donor, whereas in the previous cases, it always had the role of proton acceptor.

It is also interesting to realize that the thiomalonaldehyde-BeF₂ minima involved in the thermodynamic cycles shown in Figure 5 are interconnected through a proton transfer along the O-H...S (or S-H...O) IMHB. To analyze these processes in detail, we have evaluated the corresponding potential energy curves, where the structure of the cluster is fully optimized for the different positions of the proton that is transferred between both basic sites. The potential energy curve when BeF₂ is attached to the OH group is shown in Figure 7a, whereas the similar process along the S-H...O IMHB, when BeF₂ is attached to the S-H group, is shown in Figure 7b.

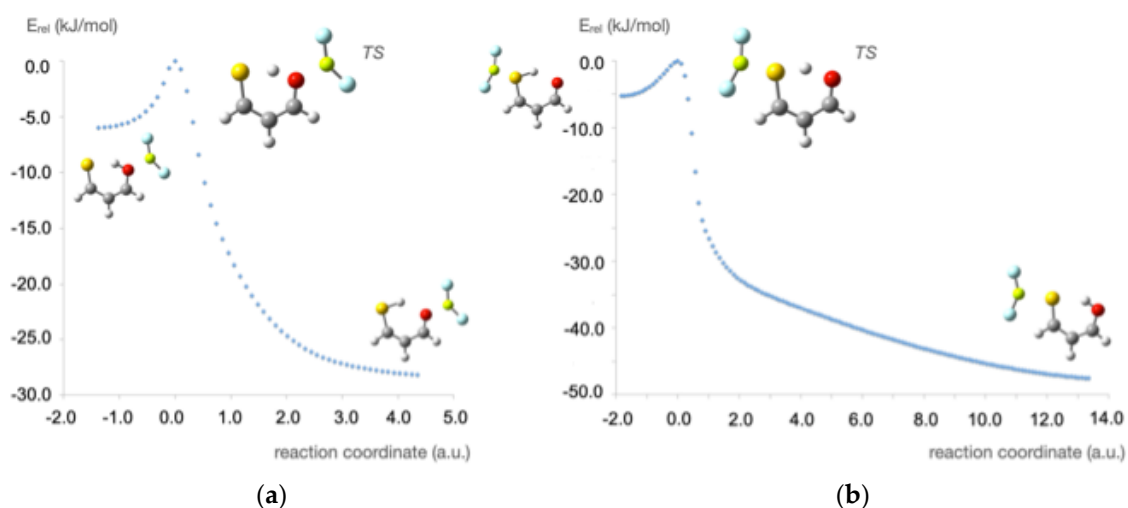


Figure 7. Potential energy curves associated to the proton transfer processes along (a) an O-H...S IMHB, with BeF₂ attached to the OH group; (b) a S-H...O IMHB, with BeF₂ attached to the SH group.

In the first case, the elongation of the O-H bond leads to a transition state (TS) which is about 5 kJ·mol⁻¹ higher than the minimum stabilized by a O-H...S IMHB. From this point, the energy of the system drops more than 25 kJ·mol⁻¹ to reach the minimum stabilized by the corresponding O...H-S IMHB. Note, however, that although the final IMHB is weaker than the initial one, the minimum reached is lower in energy than the initial one essentially due to the stronger beryllium bond. The situation is not very different in the second case. Again, the elongation of the S-H bond leads to a TS also about 5 kJ·mol⁻¹ higher than the initial minimum. From the TS, the energy of the system decreases more than 40 kJ·mol⁻¹ to reach the minimum stabilized by the corresponding S...H-O IMHB. However, in this case, both the strengthening of the IMHB and the beryllium bond are responsible for this stabilization. Indeed, the S...H-O IMHB is stronger than the S-H...O because the O-H group is a better proton donor than the S-H one, and at the same time, the new S...Be bond is also stronger than the initial HS...Be one, because the C=S group is a stronger Lewis base than the C-SH one.

3.3. $X = O, Y = NH$

If we consider now a malonaldehyde-like system combining a carbonyl and an amino group (optimized geometries in Figure S2), the shifting of one amino hydrogen to the carbonyl group leads to other two local minima as far as the pseudocyclic structures are concerned: the one in which the proton donor in the IMHB is the imino group, and the one in which the proton donor is the hydroxyl group (see the first row in Figure S2 for more details). These three possibilities are contemplated in the thermodynamic cycles shown in Figure 8. The upper part corresponds to the global minimum with a carbonyl and an amino group as functional groups. The lower part presents the results corresponding to the system stabilized by a N-H...O-H IMHB (left part) and the one stabilized by an O-H...NH IMHB (right part).

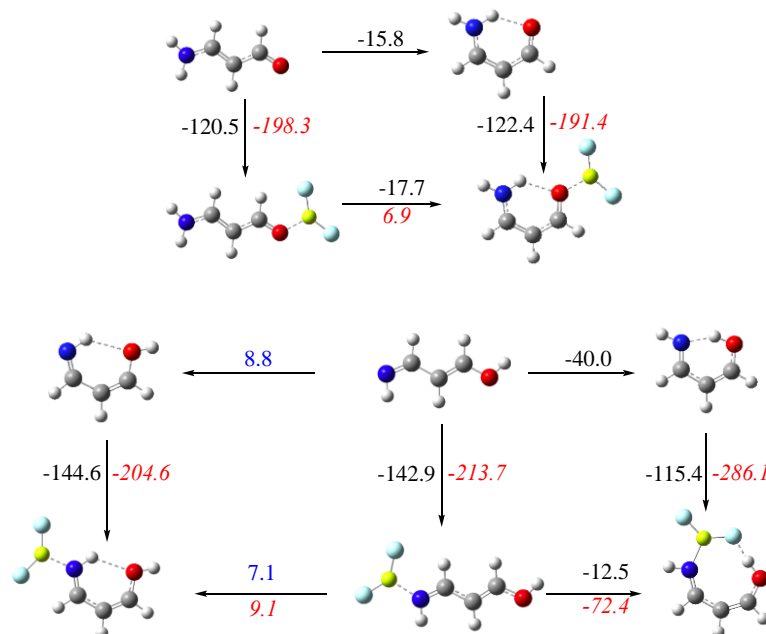


Figure 8. Thermodynamic cycles corresponding to the attachment of BeF₂ to the malonaldehyde-like in which $X = O$ and $Y = NH$. The equilibrium interaction energies are in black if the process is exothermic and in blue if it is endothermic. The diabatic interaction energies are in red. All values in kJ·mol⁻¹.

The isomer in which the IMHB proton donor is the amino group does not behave similarly to what was observed for the systems $X = Y = O$ and $X = O, Y = S$ discussed above, but similar to $X = Y = S$, showing that the cyclization of the BeF₂-cluster is more stabilizing than the cyclization of the isolated malonaldehyde-like compound, although the energy difference (1.9 kJ·mol⁻¹) is very small.

However, there are significant differences as far as the expected behavior of the enolic isomers is concerned. On the one hand, as it is illustrated in the lower part of Figure 8, when the hydrogen bond donor in the IMHB is the imino group, the formation of the pseudocyclic structure is energetically unfavorable by 8.8 kJ·mol⁻¹, and this situation does not change upon association with BeF₂, being the cyclization still unfavorable by 7.1 kJ·mol⁻¹. Conversely, when the hydrogen bond donor is the hydroxyl group, the cyclization through the formation of an IMHB is energetically very favorable (by 40 kJ·mol⁻¹). This is essentially due to the different strength of the O-H...N IMHB with respect to the N-H...O one, as shown by the electron density at the BCP, which is four times larger in the first case than in the second (see Figure S4), reflecting that the imino group is a very poor proton donor but a very good proton acceptor. The NBO analysis leads to the same conclusion, since the O-H...N IMHB second-order interaction energy between the N lone pair and the antibonding O-H orbital is about ten times greater than the interaction between the

O lone pair and the N-H antibonding orbital in the N-H...O IMHB. Consistently, in the first case, the O...N distance is 0.4 Å shorter than in the second. This cyclization upon association with BeF₂ is even more favorable in terms of diabatic interaction energies (by 72.4 kJ·mol⁻¹), because, upon attachment of BeF₂ to the imino group, the initial O-H...NH IMHB is replaced by a rather strong O-H...F IMHB. This change in the nature of the IMHB leads not only to an interaction enthalpy increase (from 102.9 to 115.4 kJ·mol⁻¹) but also to a diabatic interaction energy increase (from 213.7 to 286.1 kJ·mol⁻¹). These structural and stability changes are nicely reflected in the EDS plots (see Figure 9). Here, again, it is evident that the density redistribution induced by the beryllium bond is produced already in the linear arrangement of the system, and upon cyclization due to the formation of the O-H...F IMHB, the only significant changes are those around the F participating in the interaction, whose density is polarized toward the hydroxyl group and the density around this group itself.

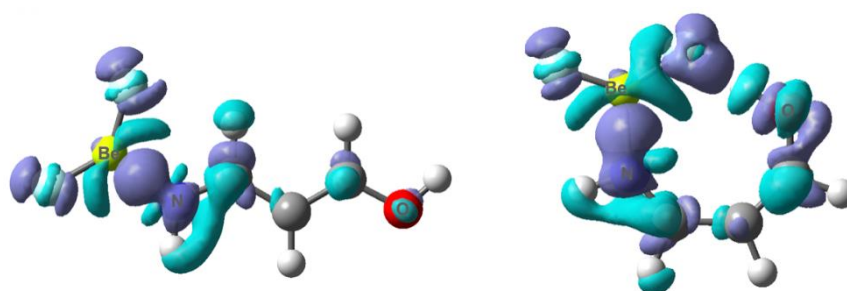


Figure 9. EDS plot for the linear and pseudocyclic conformations of the malonaldehyde-like ($X = \text{OH}$ and $Y = \text{N}$): BeF₂ cluster. Violet lobes correspond to areas in which the electron density is accumulated, whereas light blue ones correspond to areas where the electron density is depleted.

3.4. $X = \text{S}$, $Y = \text{NH}$

If oxygen is replaced by S in the previous system (optimized structures in Figure S3), the behavior observed when the hydrogen bond donor is the amino group (upper part of Figure 10) changes significantly, because now the association with BeF₂ renders the cyclization of the system energetically less favorable (9.5 vs. 19.7 kJ·mol⁻¹). This can be understood if one considers that the thiocarbonyl group is much softer than the carbonyl one, and as a consequence, sulfur is more strongly polarized toward the Be atom upon BeF₂ attachment, and therefore, a much poorer proton acceptor in the N-H...S IMHB. Consistently, upon BeF₂ attachment, the IMHB length increases 0.06 Å, and the cyclization process becomes 10.2 kJ·mol⁻¹ less exothermic.

The results obtained when the proton donor in the IMHB is the imino group (see the left thermodynamic cycle in the lower part of Figure 10) are similar to the ones discussed above for the oxygen-containing analogue, in the sense that the cyclization of the isolated system is already an endothermic process (by 12.6 kJ·mol⁻¹), and it becomes slightly more endothermic (by 15.0 kJ·mol⁻¹) upon BeF₂ attachment. Conversely, when the attachment takes place at the imino group acting as the proton donor (see the right thermodynamic cycle in the lower part of Figure 10), the situation is much different from the one discussed above for the corresponding oxygen containing analogue. The cyclization of the isolated compound is still exothermic, but when comparing Figures 8 and 10, it is clear that the exothermicity is lower (9.1 vs. 40 kJ·mol⁻¹) for the S-containing compound, because the N-H...S IMHB is weaker than the N-H...O IMHB. This is evident when looking at the molecular graphs in both cases (see Figure S4), which show that the electron density at the BCP in the first case is 0.003 a.u. smaller than in the second. Concomitantly, the NBO second-order interaction energies between the oxygen lone pair and the N-H antibonding orbital are greater than the interactions involving the sulfur lone pair.

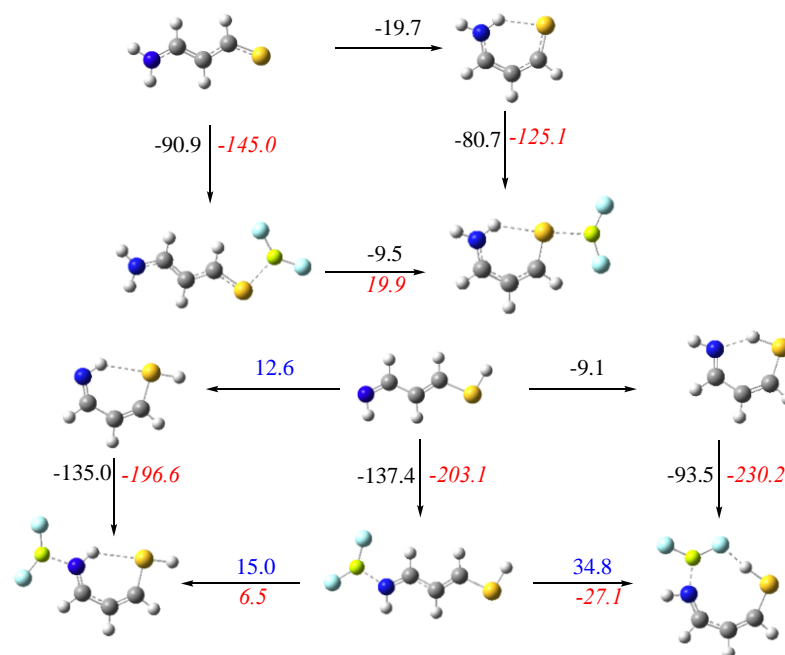


Figure 10. Thermodynamic cycles corresponding to the attachment of BeF_2 to the malonaldehyde-like in which $X = \text{S}$ and $Y = \text{NH}$. The equilibrium interaction energies are in black if the process is exothermic and in blue if it is endothermic. The diabatic interaction energies are in red. All values in $\text{kJ}\cdot\text{mol}^{-1}$.

Upon BeF_2 attachment at the imino group, acting as proton acceptor in the IMHB, the pseudocyclic cluster shows, as in the case of the oxygen-containing analogue, an IMHB with one of the F atoms of the BeF_2 moiety. However, since in this case, the proton donor is an SH group, which is a much poorer proton donor than a hydroxyl group, the IMHB is weaker (see Figure S4) and not strong enough to render the cyclization exothermic.

4. Concluding Remarks

Perhaps the most important conclusion of this survey is the different behavior exhibited by closely related systems (all of them can be generated from malonaldehyde by changing the nature of the atoms involved in the IMHB) when they form beryllium bonds with BeF_2 .

Starting with malonaldehyde, the pseudocyclic complex between it and BeF_2 is more stable than the linear one. In this pseudocyclic structure, BeF_2 is attached to carbonyl, which is the most basic site. It is worth mentioning that beryllium attached to hydroxyl leads to a stronger IMHB, but this reinforcement does not counterbalance the weakening of the beryllium bond. This fact clearly shows the importance of cooperativity. The EDS formalism revealed that resonance is already present in the linear arrangement.

Notably, the dithio analogue compound does not exhibit a significant gap between the linear and the pseudocyclic forms, indicating that in this case, the resonance-assisted phenomenon is almost inexistent, and it disappears upon BeF_2 attachment, because the formation of the beryllium bond weakens the IMHB, which is not enough to allow cyclization. This is due to the poorer sulfur abilities as a donor with respect to oxygen.

The combination of oxygen and sulfur in the malonaldehyde-like system favors cyclization when the proton donor in the IMHB is the hydroxyl group, and, even more, when Be bonds are present. This apparently surprising result is due to significant enhancement of the proton donor ability of the hydroxyl group, which is due to the charge transfer toward the BeF_2 moiety. Furthermore, the different stabilities of the isomers that can be formed reflect the different strengths of the $\text{O}\cdots\text{H}\cdots\text{S}$ IMHBs with respect to the $\text{O}\cdots\text{H}\cdots\text{S}$ ones, and

the different stability of the Be bonds when BeF₂ is attached to C=O (or C=S) groups with respect to its attachment to C-OH (or C-SH) groups.

The combination of oxygen and nitrogen in the malonaldehyde-like system also behaves differently than malonaldehyde (imine-hydroxyl isomer). We expected lower binding energies for BeF₂ in the pseudocyclic form, but not an increase on the diabatic interaction energies. The reason behind is mostly the formation of a new O-H...F IMHB. A similar situation is found for the imine-thiol isomer.

The systematic analysis of the interplay between Be bonds and IMHB combining different basic sites in malonaldehyde-like systems strongly indicates that the formation of a IMHB is not enough to predict a larger stability for the pseudocyclic forms.

Supplementary Materials: The following supporting information can be downloaded at: <https://www.mdpi.com/article/10.3390/sci4010007/s1>. Figures S1–S3: structures obtained for malonaldehyde and malonaldehyde-like systems; Figure S4: molecular graphs for some selected structures from Figure 8.

Author Contributions: Conceptualization, M.Y.; Original Draft Preparation, M.Y.; Writing, Review and Editing, M.M.M.-C., O.M. and M.Y.; Formal Analysis, M.M.M.-C., O.M. and M.Y.; Methodology, M.M.M.-C. and M.Y.; Investigation, M.M.M.-C., O.M. and M.Y.; Project Administration, O.M.; Funding Acquisition, O.M. and M.Y. All authors have read and agreed to the published version of the manuscript.

Funding: This work was carried out with financial support from the projects PGC2018-094644-B-C21, and PID2019-110091GB-I00 (MICINN) of the Ministerio de Ciencia, Innovación y Universidades of Spain.

Institutional Review Board Statement: Not applicable.

Informed Consent Statement: Not applicable.

Data Availability Statement: Not applicable.

Acknowledgments: Thanks are also given to the CTI (CSIC) and to the Centro de Computación Científica of the UAM (CCC-UAM) for the generous allocation of computer time and for their continued technical support.

Conflicts of Interest: The authors declare no conflict of interest.

References

1. Van Der Waals, J.D. *On the Continuity of the Gaseous and Liquid State*; University of Leiden: Leiden, The Netherlands, 1873.
2. Pauling, L. The Structure and Entropy of Ice and of Other Crystals with Some Randomness of Atomic Arrangement. *J. Am. Chem. Soc.* **1935**, *57*, 2680–2684. [[CrossRef](#)]
3. Latimer, W.M.; Rodebush, W.H. Polarity and ionization from the standpoint of the Lewis theory of valence. *J. Am. Chem. Soc.* **1920**, *42*, 1419–1433. [[CrossRef](#)]
4. Pauling, L.; Corey, R.B.; Branson, H.R. The structure of proteins—2 Hydrogen-bonded helical configurations of the polypeptide chain. *Proc. Natl. Acad. Sci. USA* **1951**, *37*, 205–211. [[CrossRef](#)] [[PubMed](#)]
5. Muller-Dethlefs, K.; Hobza, P. Noncovalent interactions: A challenge for experiment and theory. *Chem. Rev.* **2000**, *100*, 143–167. [[CrossRef](#)] [[PubMed](#)]
6. Hobza, P.; Zahradník, R.; Müller-Dethlefs, K. The world of non-covalent interactions: 2006. *Collect. Czech. Chem. Commun.* **2006**, *71*, 443–531. [[CrossRef](#)]
7. Hobza, P.; Müller-Dethlefs, K. *Non-Covalent Interactions. Theory and Experiment*; RSC Theoretical and Computational Chemistry Series 2; The Royal Society of Chemistry: Cambridge, UK, 2010.
8. Alkorta, I.; Elguero, J.; Frontera, A. Not Only Hydrogen Bonds: Other Noncovalent Interactions. *Crystals* **2020**, *10*, 180. [[CrossRef](#)]
9. Roza, A.O.d.I.; Dilabio, G.A. *Non-Covalent Interactions in Quantum Chemistry and Physics. Theory and Applications*; Elsevier: Amsterdam, The Netherlands, 2017.
10. Neel, A.J.; Hilton, M.J.; Sigman, M.S.; Toste, F.D. Exploiting non-covalent pi interactions for catalyst design. *Nature* **2017**, *543*, 637–646. [[CrossRef](#)]
11. Davis, H.J.; Phipps, R.J. Harnessing non-covalent interactions to exert control over regioselectivity and site-selectivity in catalytic reactions. *Chem. Sci.* **2017**, *8*, 864–877. [[CrossRef](#)]
12. Storch, G.; Trapp, O. By-design enantioselective self-amplification based on non-covalent product-catalyst interactions. *Nat. Chem.* **2017**, *9*, 179–187. [[CrossRef](#)]

13. Barnberger, J.; Ostler, F.; Mancheno, O.G. Frontiers in Halogen and Chalcogen-Bond Donor Organocatalysis. *ChemCatChem* **2019**, *11*, 5198–5211. [[CrossRef](#)]
14. Saper, N.I.; Ohgi, A.; Small, D.W.; Semba, K.; Nakao, Y.; Hartwig, J.F. Nickel-catalysed anti-Markovnikov hydroarylation of unactivated alkenes with unactivated arenes facilitated by non-covalent interactions. *Nat. Chem.* **2020**, *12*, 276–283. [[CrossRef](#)]
15. Guerra, C.F.; Bickelhaupt, F.M.; Snijders, J.G.; Baerends, E.J. The nature of the hydrogen bond in DNA base pairs: The role of charge transfer and resonance assistance. *Chem. Eur. J.* **1999**, *5*, 3581–3594. [[CrossRef](#)]
16. Guerra, C.F.; Bickelhaupt, F.M.; Snijders, J.G.; Baerends, E.J. Hydrogen bonding in DNA base pairs: Reconciliation of theory and experiment. *J. Am. Chem. Soc.* **2000**, *122*, 4117–4128. [[CrossRef](#)]
17. Cerny, J.; Hobza, P. Non-covalent interactions in biomacromolecules. *Phys. Chem. Chem. Phys.* **2007**, *9*, 5291–5303. [[CrossRef](#)] [[PubMed](#)]
18. Cockroft, S.L.; Hunter, C.A. Chemical double-mutant cycles: Dissecting non-covalent interactions. *Chem. Soc. Rev.* **2007**, *36*, 172–188. [[CrossRef](#)] [[PubMed](#)]
19. Riley, K.E.; Hobza, P. Noncovalent interactions in biochemistry. *WIREs Comput. Mol. Sci.* **2011**, *1*, 3–17. [[CrossRef](#)]
20. Maharramov, A.M.; Mahmudov, K.T.; Kopylovich, M.N.; Pombeiro, A.J.L. *Non-covalent Interactions in the Synthesis and Design of New Compounds*; John Wiley & Sons: Hoboken, NJ, USA, 2016.
21. Biedermann, F.; Schneider, H.J. Experimental Binding Energies in Supramolecular Complexes. *Chem. Rev.* **2016**, *116*, 5216–5300. [[CrossRef](#)] [[PubMed](#)]
22. Berger, G.; Frangville, P.; Meyer, F. Halogen bonding for molecular recognition: New developments in materials and biological sciences. *Chem. Comm.* **2020**, *56*, 4970–4981. [[CrossRef](#)]
23. Sarkar, A.; Behera, T.; Sasmal, R.; Capelli, R.; Empereur-mot, C.; Mahato, J.; Agasti, S.S.; Pavan, G.M.; Chowdhury, A.; George, S.J. Cooperative Supramolecular Block Copolymerization for the Synthesis of Functional Axial Organic Heterostructures. *J. Am. Chem. Soc.* **2020**, *142*, 11528–11539. [[CrossRef](#)]
24. Bauzá, A.; Frontera, A. Aerogen Bonding Interaction: A New Supramolecular Force? *Angew. Chem. Int. Ed.* **2015**, *54*, 7340–7343. [[CrossRef](#)]
25. Cavallo, G.; Metrangolo, P.; Milani, R.; Pilati, T.; Priimagi, A.; Resnati, G.; Terraneo, G. The Halogen Bond. *Chem. Rev.* **2016**, *116*, 2478–2601. [[CrossRef](#)] [[PubMed](#)]
26. Desiraju, G.R.; Ho, P.S.; Kloo, L.; Legon, A.C.; Marquardt, R.; Metrangolo, P.; Politzer, P.; Resnati, G.; Rissanen, K. Definition of the halogen bond (IUPAC Recommendations 2013). *Pure Appl. Chem.* **2013**, *85*, 1711–1713. [[CrossRef](#)]
27. Wang, W.; Ji, B.; Zhang, Y. Chalcogen Bond: A Sister Noncovalent Bond to Halogen Bond. *J. Phys. Chem. A* **2009**, *113*, 8132–8135. [[CrossRef](#)]
28. Sanz, P.; Yáñez, M.; Mó, O. Competition between X···H···Y Intramolecular Hydrogen Bonds and X···Y (X = O, S, and Y = Se, Te) Chalcogen-Chalcogen Interactions. *J. Phys. Chem. A* **2002**, *106*, 4661–4668. [[CrossRef](#)]
29. Alkorta, I.; Rozas, I.; Elguero, J. Molecular Complexes between Silicon Derivatives and Electron-Rich Groups. *J. Phys. Chem. A* **2001**, *105*, 743–749. [[CrossRef](#)]
30. Aakeroy, C.B.; Bryce, D.L.; Desiraju, G.R.; Frontera, A.; Legon, A.C.; Nicotra, F.; Rissanen, K.; Scheiner, S.; Terraneo, G.; Metrangolo, P.; et al. Definition of the chalcogen bond (IUPAC Recommendations 2019). *Pure Appl. Chem.* **2019**, *91*, 1889. [[CrossRef](#)]
31. Grabowski, S.J. Tetrel bond-sigma-hole bond as a preliminary stage of the S(N)2 reaction. *Phys. Chem. Chem. Phys.* **2014**, *16*, 1824–1834. [[CrossRef](#)]
32. Bauzá, A.; Mooibroek, T.J.; Frontera, A. Tetrel-Bonding Interaction: Rediscovered Supramolecular Force? *Angew. Chem. Int. Ed.* **2013**, *52*, 12317–12321. [[CrossRef](#)]
33. Grabowski, S.J. Boron and other Tritel Lewis Acid Centers: From Hypovalency to Hypervalency. *ChemPhysChem* **2014**, *15*, 2985–2993. [[CrossRef](#)]
34. Alkorta, I.; Elguero, J.; Del Bene, J.E.; Mó, O.; Yáñez, M. New Insights into Factors Influencing B-N Bonding in X: BH₃-nFn and X: BH₃-nCl_n for X = N-2, HCN, LiCN, H₂CNH, NF₃, NH₃ and n = 0-3: The Importance of Deformation. *Chem. Eur. J.* **2010**, *16*, 11897–11905. [[CrossRef](#)]
35. Bauzá, A.; Alkorta, I.; Elguero, J.; Mooibroek, T.J.; Frontera, A. Spodium Bonds: Noncovalent Interactions Involving Group 12 Elements. *Angew. Chem. Int. Ed.* **2020**, *59*, 17482–17487. [[CrossRef](#)] [[PubMed](#)]
36. Legon, A.C.; Walker, N.R. What's in a name? 'Coinage-metal' non-covalent bonds and their definition. *Phys. Chem. Chem. Phys.* **2018**, *20*, 19332–19338. [[CrossRef](#)] [[PubMed](#)]
37. Sánchez-Sanz, G.; Trujillo, C.; Alkorta, I.; Elguero, J. Understanding Regium Bonds and their Competition with Hydrogen Bonds in Au₂:HX Complexes. *ChemPhysChem* **2019**, *20*, 1572–1580. [[CrossRef](#)] [[PubMed](#)]
38. Zierkiewicz, W.; Michalczyk, M.; Scheiner, S. Regium bonds between Mn clusters (M = Cu, Ag, Au and n = 2–6) and nucleophiles NH₃ and HCN. *Phys. Chem. Chem. Phys.* **2018**, *20*, 22498–22509. [[CrossRef](#)] [[PubMed](#)]
39. Stenlid, J.H.; Brinck, T. Extending the σ-Hole Concept to Metals: An Electrostatic Interpretation of the Effects of Nanostructure in Gold and Platinum Catalysis. *J. Am. Chem. Soc.* **2017**, *139*, 11012–11015. [[CrossRef](#)]
40. Alkorta, I.; Legon, A.C. Non-Covalent Interactions Involving Alkaline-Earth Atoms and Lewis Bases B: An ab Initio Investigation of Beryllium and Magnesium Bonds, B···MR₂ (M = Be or Mg, and R = H, F or CH₃). *Inorganics* **2019**, *7*, 35. [[CrossRef](#)]

41. M6, O.; Montero-Campillo, M.M.; Alkorta, I.; Elguero, J.; Y6,nez, M. Ternary Complexes Stabilized by Chalcogen and Alkaline-Earth Bonds: Crucial Role of Cooperativity and Secondary Noncovalent Interactions. *Chem. Eur. J.* **2019**, *25*, 11688–11695. [[CrossRef](#)]
42. Alkorta, I.; Hill, J.G.; Legon, A.C. An ab initio investigation of alkali–metal non-covalent bonds $B \cdots LiR$ and $B \cdots NaR$ ($R = F, H$ or CH_3) formed with simple Lewis bases B : The relative inductive effects of F, H and CH_3 . *Phys. Chem. Chem. Phys.* **2020**, *22*, 16421–16430. [[CrossRef](#)]
43. Y6,nez, M.; Sanz, P.; M6, O.; Alkorta, I.; Elguero, J. Beryllium Bonds, do they exist? *J. Chem. Theor. Comput.* **2009**, *5*, 2763–2771. [[CrossRef](#)]
44. Montero-Campillo, M.M.; M6, O.; Y6,nez, M.; Alkorta, I.; Elguero, J. The Beryllium Bond. In *Advances in Inorganic Chemistry*; VanEldik, R., Puchta, R., Eds.; Elsevier: San Diego, CA, USA; Academic Press, Inc.: Cambridge, MA, USA, 2019; Volume 73, pp. 73–121.
45. Albrecht, L.; Boyd, R.J.; M6, O.; Y6,nez, M. Changing Weak Halogen Bonds into Strong Ones through Cooperativity with Beryllium Bonds. *J. Phys. Chem. A* **2014**, *118*, 4205–4213. [[CrossRef](#)]
46. McDowell, S.A.C.; Hamilton, D.S. Cooperative effects of hydrogen, halogen and beryllium bonds on model halogen-bonded $FX \cdots YZ$ ($YZ = BF, CO, N_2$) complexes in $FX' \cdots FCl \cdots YZ$ trimers ($FX' = FH, FCl, F_2Be$). *Mol. Phys.* **2015**, *113*, 1991–1997. [[CrossRef](#)]
47. Yu, D.; Wu, D.; Li, Y.; Li, S.Y. On the formation of beryllium bonds where radicals act as electron donors. *Theor. Chem. Acc.* **2016**, *135*. [[CrossRef](#)]
48. Bauz6, A.; Frontera, A. On the Importance of π -Hole Beryllium Bonds: Theoretical Study and Biological Implications. *Chem. Eur. J.* **2017**, *23*, 5375–5380. [[CrossRef](#)] [[PubMed](#)]
49. Casals-Sainz, J.L.; Jim6,nez-Gr6,valos, F.; Costales, A.; Francisco, E.; Pend6,as, A.M. Beryllium Bonding in the Light of Modern Quantum Chemical Topology Tools. *J. Phys. Chem. A* **2018**, *122*, 849–858. [[CrossRef](#)]
50. Alikhani, M.E. Beryllium bonding: Insights from the sigma- and pi-hole analysis. *J. Mol. Model.* **2020**, *26*, 94. [[CrossRef](#)]
51. Alkorta, I.; Blanco, F.; Dey6, P.M.; Elguero, J.; Estarellas, C.; Frontera, A.; Qui6,nero, D. Cooperativity in multiple unusual weak bonds. *Theor. Chem. Acc.* **2010**, *126*, 1–14. [[CrossRef](#)]
52. Mahadevi, A.S.; Sastry, G.N. Cooperativity in Noncovalent Interactions. *Chem. Rev.* **2016**, *116*, 2775–2825. [[CrossRef](#)]
53. M6, O.; Y6,nez, M.; Elguero, J. Cooperative (nonpairwise) effects in water trimers: An ab initio molecular orbital study. *J. Chem. Phys.* **1992**, *97*, 6628–6638. [[CrossRef](#)]
54. Albrecht, L.; Boyd, R.J. Atomic energy analysis of cooperativity, anti-cooperativity, and non-cooperativity in small clusters of methanol, water, and formaldehyde. *Comp. Theor. Chem.* **2015**, *1053*, 328–336. [[CrossRef](#)]
55. Adasme-Carreno, F.; Alzate-Morales, J.; Ireta, J. Modeling cooperative effects in halogen-bonded infinite linear chains. *Phys. Chem. Chem. Phys.* **2017**, *19*, 18529–18538. [[CrossRef](#)]
56. Roman, M.; Cannizzo, C.; Pinault, T.; Isare, B.; Andrioletti, B.; van der Schoot, P.; Bouteiller, L. Supramolecular Balance: Using Cooperativity to Amplify Weak Interactions. *J. Am. Chem. Soc.* **2010**, *132*, 16818–16824. [[CrossRef](#)] [[PubMed](#)]
57. Grabowski, S.J. Cooperativity of hydrogen and halogen bond interactions. *Theor. Chem. Acc.* **2013**, *132*, 10. [[CrossRef](#)]
58. Domagala, M.; Lutynska, A.; Palusiak, M. Halogen bond versus hydrogen bond: The many-body interactions approach. *Int. J. Quant. Chem.* **2017**, *117*, e25348. [[CrossRef](#)]
59. Ciancaleoni, G. Cooperativity between hydrogen- and halogen bonds: The case of selenourea. *Phys. Chem. Chem. Phys.* **2018**, *20*, 8506–8514. [[CrossRef](#)]
60. Yang, J.; Yu, Q.; Yang, F.-L.; Lu, K.; Yan, C.-X.; Dou, W.; Yang, L.; Zhou, P.-P. Competition and cooperativity of hydrogen-bonding and tetrel-bonding interactions involving triethylene diamine (DABCO), H_2O and CO_2 in air. *New J. Chem.* **2020**, *44*, 2328–2338. [[CrossRef](#)]
61. Hou, M.C.; Zhu, Y.F.; Li, Q.Z.; Scheiner, S. Tuning the Competition between Hydrogen and Tetrel Bonds by a Magnesium Bond. *Chemphyschem* **2020**, *21*, 212–219. [[CrossRef](#)]
62. Liu, M.; Yang, L.; Li, Q.; Li, W.; Cheng, J.; Xiao, B.; Yu, X. Modulating the strength of tetrel bonding through beryllium bonding. *J. Mol. Model.* **2016**, *22*, 192. [[CrossRef](#)]
63. George, J.; Deringer, V.L.; Dronskowski, R. Cooperativity of Halogen, Chalcogen, and Pnictogen Bonds in Infinite Molecular Chains by Electronic Structure Theory. *J. Phys. Chem. A* **2014**, *118*, 3193–3200. [[CrossRef](#)]
64. Alkorta, I.; Elguero, J.; Del Bene, J.E.; M6, O.; Montero-Campillo, M.M.; Y6,nez, M. Mutual Influence of Pnictogen Bonds and Beryllium Bonds: Energies and Structures in the Spotlight. *J. Phys. Chem. A* **2020**, *124*, 5871–5878. [[CrossRef](#)]
65. Albrecht, L.; Boyd, R.J.; M6, O.; Y6,nez, M. Cooperativity between hydrogen bonds and beryllium bonds in $(H_2O)_n BeX_2$ ($n=1-3$, $X = H, F$) complexes. A new perspective. *Phys. Chem. Chem. Phys.* **2012**, *14*, 14540–14547. [[CrossRef](#)]
66. Gilli, G.; Bellucci, F.; Ferretti, V.; Bertolasi, V. Evidence for resonance-assisted hydrogen-bonding from crystal-structure correlations on the enol form of the beta-diketone fragment. *J. Am. Chem. Soc.* **1989**, *111*, 1023–1028. [[CrossRef](#)]
67. Curtiss, L.A.; Redfern, P.C.; Raghavachari, K. Gaussian-4 theory. *J. Chem. Phys.* **2007**, *126*, 84108. [[CrossRef](#)] [[PubMed](#)]
68. Moller, C.; Plesset, M.S. Note on an approximation treatment for many-electron systems. *Phys. Rev.* **1934**, *46*, 0618–0622. [[CrossRef](#)]
69. Krishnan, R.; Pople, J.A. Approximate 4th-order perturbation-theory of electron correlation energy. *Int. J. Quant. Chem.* **1978**, *14*, 91–100. [[CrossRef](#)]
70. Raghavachari, K.; Trucks, G.W.; Pople, J.A.; Headgordon, M. A 5th-order perturbation comparison of electron correlation theories. *Chem. Phys. Lett.* **1989**, *157*, 479–483. [[CrossRef](#)]

71. Bader, R.F.W. *Atoms in Molecules. A Quantum Theory*; Clarendon Press: Oxford, UK, 1990.
72. Reed, A.E.; Curtiss, L.A.; Weinhold, F. Intermolecular interactions from a natural bond orbital, donor-acceptor viewpoint. *Chem. Rev.* **1988**, *88*, 899–926. [[CrossRef](#)]
73. Sánchez-Sanz, G.; Trujillo, C.; Alkorta, I.; Elguero, J. Electron density shift description of non-bonding intramolecular interactions. *Comput. Theor. Chem.* **2012**, *991*, 124–133. [[CrossRef](#)]
74. Wiberg, K.B. Application of pople-santry-segal cndo method to cyclopropylcarbinyl and cyclobutyl cation and to bicyclobutane. *Tetrahedron* **1968**, *24*, 1083–1088. [[CrossRef](#)]
75. Iribarren, I.; Sánchez-Sanz, G.; Alkorta, I.; Elguero, J.; Trujillo, C. Evaluation of Electron Density Shifts in Noncovalent Interactions. *J. Phys. Chem. A* **2021**, *125*, 4741–4749. [[CrossRef](#)]
76. Alkorta, I.; Elguero, J.; Mó, O.; Yáñez, M.; Del Bene, J.E. Do coupling constants and chemical shifts provide evidence for the existence of resonance-assisted hydrogen bonds? *Mol. Phys.* **2004**, *102*, 2563–2574. [[CrossRef](#)]
77. Alkorta, I.; Elguero, J.; Mó, O.; Yáñez, M.; Del Bene, J.E. Are resonance-assisted hydrogen bonds ‘resonance assisted’? A theoretical NMR study. *Chem. Phys. Lett.* **2005**, *411*, 411–415. [[CrossRef](#)]
78. Kurczab, R.; Mitoraj, M.P.; Michalak, A.; Ziegler, T. Theoretical Analysis of the Resonance Assisted Hydrogen Bond Based on the Combined Extended Transition State Method and Natural Orbitals for Chemical Valence Scheme. *J. Phys. Chem. A* **2010**, *114*, 8581–8590. [[CrossRef](#)] [[PubMed](#)]
79. Gora, R.W.; Maj, M.; Grabowski, S.J. Resonance-assisted hydrogen bonds revisited. Resonance stabilization vs. charge delocalization. *Phys. Chem. Chem. Phys.* **2013**, *15*, 2514–2522. [[CrossRef](#)] [[PubMed](#)]
80. Guevara-Vela, J.M.; Romero-Montalvo, E.; del Rio-Lima, A.; Martin Pendas, A.; Hernandez-Rodriguez, M.; Rinza, T.R. Hydrogen-Bond Weakening through pi Systems: Resonance-Impaired Hydrogen Bonds (RIHB). *Chem. Eur. J.* **2017**, *23*, 16605–16611. [[CrossRef](#)] [[PubMed](#)]
81. Grosch, A.A.; van der Lubbe, S.C.C.; Guerra, C.F. Nature of Intramolecular Resonance Assisted Hydrogen Bonding in Malonaldehyde and Its Saturated Analogue. *J. Phys. Chem. A* **2018**, *122*, 1813–1820. [[CrossRef](#)] [[PubMed](#)]
82. Guevara-Vela, J.M.; Gallegos, M.; Valentin-Rodriguez, M.A.; Costales, A.; Rocha-Rinza, T.; Pendas, A.M. On the Relationship between Hydrogen Bond Strength and the Formation Energy in Resonance-Assisted Hydrogen Bonds. *Molecules* **2021**, *26*, 4196. [[CrossRef](#)]